ESANN 2022 proceedings, European Symposium on Artificial Neural Networks, Computational Intelligence and Machine Learning. Bruges (Belgium) and online event, 5-7 October 2022, i6doc.com publ., ISBN 978287587084-1. Available from http://www.i6doc.com/en/.

Adaptive Gabor Filters for Interpretable Color Texture Classification

Gerrit Luimstra and Kerstin Bunte

University of Groningen - Science and Engineering
Nijenborgh 9, Groningen - Netherlands

Abstract. We introduce the use of trainable feature extractors, based on the Gabor function, into the interpretable machine learning domain. The use of adaptive Gabor filters allows for interpretable feature extraction to be learned automatically in a domain agnostic way, and comes with the benefit of a large reduction in trainable parameters. We implemented the filters into an image classification variant of learning vector quantization We extend and compare the image classification variant of learning vector quantization with adaptive Gabor filters and demonstrate the proposed technique on VisTex color texture images. The adaptive Gabor filters show promising results for interpretable and efficient color texture classification.

1 Introduction

A Gabor filter is a linear spatial filter often used as a feature extractor in traditional image analysis and pattern recognition tasks. Their response patterns have been investigated and compared to receptive fields in the visual cortex [1, 2, 3, 4], and Gabor filters are shown to be a good model for the structure of simple cells in cats [2, 5]. For this reason, many attempts have been made to incorporate Gabor filter-based feature extractors into machine learning pipelines [6, 7, 8, 9]. Recently, it is stated that *approximations* of Gabor filters are almost always found in the first layer of state-of-the-art convolutional neural network (CNN) architectures [10]. Therefore, it appears that Gabor filters are ubiquitous in high-performance image classification solutions, either directly or indirectly.

Due to the recent successes in applying CNNs to image classification tasks [11, 12, 13, 14] and their superior performance over traditional methods in domains where lots of data is available, many machine learning practitioners have started using such networks in a variety of settings. The power of neural networks comes from the fact that they equip learnable feature extractors formed by the networks themselves, cutting out the need of a costly human design process at the expense of high computational costs and the need for a large dataset. However, since the output of these networks is a composition of several layers, consisting of many connected units (often totalling millions of elements), the resulting outputs are often not directly interpretable.

To aid CNNs with the learning of robust and data-agnostic feature extractors, Gabor filters were recently incorporated into the architectures directly [15, 16]. However, the outputs of the resulting model will still be difficult to interpret. Learning vector quantization (LVQ) models with adaptive dissimilarities on the other hand provide efficient transparent decisions while preserving classification performance [17, 18, 19]. In this contribution we extend color image analysis LVQ (CIA-LVQ) [18, 19] to incorporate adaptive Gabor filters. The resulting model

ESANN 2022 proceedings, European Symposium on Artificial Neural Networks, Computational Intelligence and Machine Learning. Bruges (Belgium) and online event, 5-7 October 2022, i6doc.com publ., ISBN 978287587084-1. Available from http://www.i6doc.com/en/.

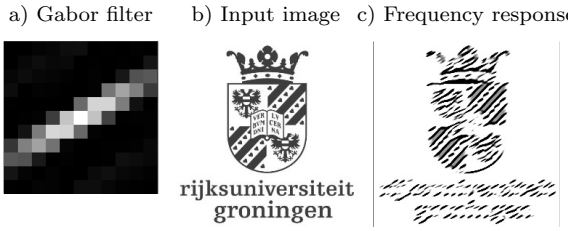

Fig. 1: Visualization of Gabor filter (a) with $\theta = \frac{\pi}{3}$ and $\lambda = 5$ convolved with the RuG logo as input (b) and resulting frequency response (c).

greatly reduces the numbers of free parameters for optimization, while preserving interpretation in form of class specific Gabor filter banks. Its performance is demonstrated on Vistex color texture images and is comparable or superior to the general convolution version. The code is available at `https://git.lwp.rug.nl/k.bunte/cialvq_luimstra`.

2 Methods

2.1 Gabor Filter

A 2D real-valued Gabor filter often used in texture analysis [6] is defined as:

$$\mathbf{g}_{\mathbf{\Theta}}(x, y) = \exp\left(-(x'^2 + \gamma^2 y'^2)/2\sigma^2\right) \cos\left(2\pi x'/\lambda + \phi\right) \quad . \tag{1}$$

where x, y denote the pixel positions, $\mathbf{\Theta} = \{\theta, \lambda, \phi, \sigma, \gamma\}$ the set of filter parameters and for short $x' = x\cos(\theta) + y\sin(\theta)$ and $y' = -x\sin(\theta) + y\cos(\theta)$. The Gabor filter response depends on the choice of parameters. In essence, θ denotes rotation (orientation) with values between 0 and 2π. The λ parameter denotes wavelength of the cosine factor with a respective domain of all real numbers greater than 2, and σ determines the size. The ratio σ/λ denotes the spatial frequency bandwidth b of simple cells as shown in Neurophysiological research: $\sigma/\lambda = 1/\pi\sqrt{\ln 2/2}2^b + 1/2^b - 1 \implies \sigma = \lambda/\pi\sqrt{\ln 2/2}2^b + 1/2^b - 1$ and therefore should not be specified directly [20]. $\phi \in [-\pi, \pi]$ denotes the phase offset of the cosine factor and determines the symmetry. Finally, $\gamma \in [0, 1]$ controls the degree of deviation from circularity (spatial aspect ratio). Fig. 1a shows an example 2D Gabor filter with $\mathbf{\Theta} = \{\pi/3, 5, 0, 2.4, 3/4\}$ that excites in presence of diagonal lines of an angle close to θ. Panel b and c depict an example input image and the corresponding filter response, that highlight these diagonals.

2.2 Real-valued Color Image Analysis LVQ (RCIA-LVQ)

The real-valued Color Image Analysis LVQ (RCIA-LVQ) bases on the original CIA-LVQ algorithm [18, 19] restricted to real-valued inputs rather than complex values. We assume a dataset $\mathcal{D}$ consisting of three channel color patches (such as RGB), as vectorized input samples $\mathbf{x}^i \in \mathbb{R}^{p \cdot p \cdot 3}$, with corresponding labels $y^i \in \{1, \ldots, C\}$ for the C class classification problem. Furthermore, a filter bank $\mathbf{G}^j$ is initialized as sum of a fixed number of Gabor filters of different parameterizations. The LVQ model consists of $K \geq C$ prototypes $\mathbf{w}^j \in \mathbb{R}^{p \cdot p}$ with $j \in \{1, \ldots, K\}$ and their respective class label $c(\mathbf{w}^j) \in \{1, \ldots, C\}$. A set of K image descriptors $\mathbf{r}^j : \mathbb{R}^{p \cdot p \cdot 3} \to \mathbb{R}^{p \cdot p}$ map the vectorized three channel input image $\mathbf{x}^i$ to a single "intensity" channel using an adaptive transformation matrix

ESANN 2022 proceedings, European Symposium on Artificial Neural Networks, Computational Intelligence and Machine Learning. Bruges (Belgium) and online event, 5-7 October 2022, i6doc.com publ., ISBN 978287587084-1. Available from http://www.i6doc.com/en/.

$\mathbf{\Omega}_j \in \mathbb{R}^{p \cdot p \times p \cdot p \cdot 3}$ and then convolve the result with the filter bank $\mathbf{G}^j$:

$$\mathbf{r}^j(\mathbf{x}^i) = \mathbf{x}^i \mathbf{\Omega}_j^T * \mathbf{G}^j \tag{2}$$

where $*$ denotes convolution, and j is the index of the associated prototype $\mathbf{w}^j$. Eq. (2) presents the most complex version with each prototype possessing a local adaptive transformation and filter bank. We furthermore implemented less complex special cases, namely the global version in which all prototypes share the same transformation $\mathbf{\Omega}$ but local filter banks $\mathbf{G}^j$ and class-wise ones $\mathbf{\Omega}_c$ and local $\mathbf{G}^j$ where c corresponds to the class of the respective prototype. The dissimilarity between an image descriptor $\mathbf{r}^j(\mathbf{x}^i)$ and a prototype $\mathbf{w}^j$ is:

$$d(\mathbf{x}^i, \mathbf{w}^j) = \|(\mathbf{r}^j(\mathbf{x}^i))^2 - (\mathbf{w}^j)^2\|^2 \ . \tag{3}$$

The class label of the closest prototype $\arg\min_j(d(\mathbf{x}^i, \mathbf{w}^j))$ is used to classify samples. For optimization of the RCIA-LVQ model parameters the following cost function is minimized, for example with stochastic gradient descent:

$$\mathcal{L}(\mathcal{D}) = \sum_i \frac{d(\mathbf{x}^i, \mathbf{w}^J) - d(\mathbf{x}^i, \mathbf{w}^K)}{d(\mathbf{x}^i, \mathbf{w}^J) + d(\mathbf{x}^i, \mathbf{w}^J)} \ , \tag{4}$$

where $\mathbf{w}^J$ denotes the closest prototype with the same class label ($c(\mathbf{w}^J) = y^i$) and $\mathbf{w}^K$ the closest non-matching prototype ($c(\mathbf{w}^K) \neq y^i$). The learning rules of the RCIA-LVQ can be derived analogous to CIA-LVQ [18, 19] by taking the partial derivatives of $\mathcal{L}$ with respect to the parameters $\mathbf{w}^L$, $\mathbf{\Omega}_L$ and $\mathbf{G}^L$, where $L \in \{J, K\}$ refers to the closest matching and non-matching prototype:

$$\begin{aligned}
\frac{\partial \mathcal{L}}{\partial \mathbf{w}^L} &= -4 \cdot \Gamma^L \left[\left(\left(\mathbf{r}^L(\mathbf{x}^i)\right)^2 - \left(\mathbf{w}^L\right)^2 \right) \cdot \mathbf{w}^L \right] \ , \\
\frac{\partial \mathcal{L}}{\partial \mathbf{\Omega}_L} &= 4 \cdot \Gamma^L \left[\left(\left(\mathbf{r}^L(\mathbf{x}^i)\right)^2 - \left(\mathbf{w}^L\right)^2 \right) * (\mathbf{G}^L)^2 \cdot \left(\mathbf{x}^i \mathbf{\Omega}_L^T \right) \mathbf{x}^{i^T} \right] \ , \\
\frac{\partial \mathcal{L}}{\partial \mathbf{G}^L} &= 4 \cdot \Gamma^L \left[\left(\left(\mathbf{r}^j(\mathbf{x}^i)\right)^2 - \left(\mathbf{w}^L\right)^2 \right) \cdot \left(\mathbf{x}^i \mathbf{\Omega}_L^T \right)^2 \right] \cdot \mathbf{G}^L \text{ with} \\
\Gamma^J &= \frac{2 \cdot d\left(\mathbf{x}^i, \mathbf{w}^K\right)}{\left(d\left(\mathbf{x}^i, \mathbf{w}^J\right) + d\left(\mathbf{x}^i, \mathbf{w}^K\right)\right)^2} \quad \text{and} \quad \Gamma^K = \frac{-2 \cdot d\left(\mathbf{x}^i, \mathbf{w}^J\right)}{\left(d\left(\mathbf{x}^i, \mathbf{w}^J\right) + d\left(\mathbf{x}^i, \mathbf{w}^K\right)\right)^2} \ .
\end{aligned}$$

2.3 Adaptive Gabor RCIA-LVQ (GaRCIA-LVQ)

In the definition of RCIA-LVQ the filter bank $\mathbf{G}^j$ does not remain a sum of Gabor filters when updated, but instead becomes a generalized convolutional kernel. To constrain the bank to ascertain the sum of Gabor filters our new bank is defined as sum of adaptive Gabor filters parameterized by sets $\widehat{\mathbf{\Theta}}_l^j$: $\widehat{\mathbf{G}}^j = \sum_l \mathbf{g}_{\widehat{\mathbf{\Theta}}_l^j}(x, y)$. This effectively reduces the number of adaptable parameters in a filter bank $\mathbf{G}^j$ from $\mathcal{O}(l \cdot p^2)$ to $\mathcal{O}(l \cdot 5)$, where p denotes the width and height of the filter and l denotes the amount of filters in the Gabor filter bank. It should be noted that this specification has the additional benefit of being invariant to filter size as an increase of filter size does not increase the number of adaptable parameters.

ESANN 2022 proceedings, European Symposium on Artificial Neural Networks, Computational Intelligence and Machine Learning. Bruges (Belgium) and online event, 5-7 October 2022, i6doc.com publ., ISBN 978287587084-1. Available from http://www.i6doc.com/en/.

We call this new version the Gabor RCIA-LVQ (GaRCIA-LVQ). Most of the derivatives remain the same, but the one with respect to $\widehat{\mathbf{G}}^j$ changes. Instead of updating the individual kernel weights the derivative is taken with respect to the parameters of the sets $\widehat{\mathbf{\Theta}}_l^j$. The partial derivative can be written as:

$$\frac{\partial \mathcal{L}}{\partial \widehat{\mathbf{\Theta}}_{l\xi}^L} = 4\Gamma^L \left[\left(\left(\mathbf{r}^L(\mathbf{x}^i)\right)^2 - \left(\mathbf{w}^L\right)^2 \right) \cdot \left(\mathbf{x}^i \mathbf{\Omega}_L^T\right)^2 \right] \cdot \widehat{\mathbf{G}}_l^L \cdot \sum_{x,y} \frac{\partial \mathbf{g}_{\widehat{\mathbf{\Theta}}_l^L}(x,y)}{\partial \xi} \quad , \tag{5}$$

where $\xi \in \{\theta, \lambda, \phi, b, \gamma\}$ denotes the filter parameter with corresponding derivatives:

$$\frac{\partial \mathbf{g}(x,y)}{\partial b} = \mathbf{g}(x,y)\frac{\lambda}{\pi}\sqrt{\frac{\ln 2}{2}}\frac{\left(x'^2 - \gamma^2 y'^2\right)\left(2^{b+1}\ln(2)\right)}{2\sigma^3(2^b-1)^2}$$

$$\frac{\partial \mathbf{g}(x,y)}{\partial \phi} = -\Psi \qquad \frac{\partial \mathbf{g}(x,y)}{\partial \lambda} = \Psi \frac{2\pi x'^2}{\lambda^2}$$

$$\frac{\partial \mathbf{g}(x,y)}{\partial \gamma} = -\mathbf{g}(x,y)\frac{\gamma y'^2}{\sigma^2} \qquad \frac{\partial \mathbf{g}(x,y)}{\partial \theta} = -\Psi \frac{2\pi y'}{\lambda} + \frac{\mathbf{g}(x',y')}{\sigma^2}(\gamma^2 - 1) \quad ,$$

where $\Psi = \exp\left(-\frac{x'^2+\gamma^2 y'^2}{2\sigma^2}\right)\sin\left(2\pi\frac{x'}{\lambda} + \phi\right)$.

3 Experiments and Results

In this section we compare and analyze the performance of the new adaptive Gabor filter bank GaRCIA-LVQ to the RCIA-LVQ with static bank as well as local and class-wise transformations and filters. The VisTex [21] database is a collection of texture images and was created with the intention of providing a large set of high quality textures for computer vision applications. The images in VisTex do not conform to rigid frontal plane perspectives and studio lighting conditions and hence are considered representative of real world conditions. Similar to [19] we use the same subset 29 images with size 128 by 128 pixels from the groups Bark, Brick, Fabric and Food as exemplified in figure 2, in order to make the performance directly comparable.

For evaluation the global training set of 29 images is randomly split into a train set of 16 and hold-out test set of 13 images. Note that the latter only serves for final evaluation and is not used for model training or selection. From each image in the training set 200 patches of size 15 by 15 are extracted and 50 patches of the same size for the hold-out test set resulting in 3200 and 650 data samples respectively. We then further split the training set into 4 folds and

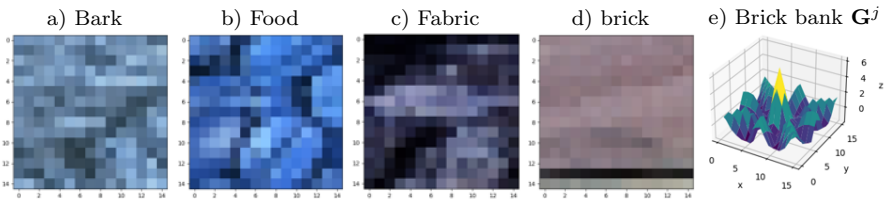

Fig. 2: a) - d) Four example images of the four classes used of the VisTex data (size 15 by 15). e) Example of a learned Gabor filter bank for the Brick class.

ESANN 2022 proceedings, European Symposium on Artificial Neural Networks, Computational Intelligence and Machine Learning. Bruges (Belgium) and online event, 5-7 October 2022, i6doc.com publ., ISBN 978287587084-1. Available from http://www.i6doc.com/en/.

Table 1: VisTex performance results. $\mathbf{\Omega}$ indicates which type of transformation matrices are used and k describes the amount of prototypes. The final columns denote the validation, train and test accuracy, respectively.

Algorithm	$\mathbf{\Omega}$	k	**Validation** ($\mu \pm \sigma$)	**Train**	**Test**
(Static) RCIA	LC	3	80.1 ± 1.9	96.7	82.0
RCIA	LC	1	80.0 ± 0.2	89.5	80.3
RCIA	LC	3	83.1 ± 0.9	**98.9**	84.9
RCIA	LC	5	$\mathbf{84.8 \pm 1.6}$	98.5	87.8
GaRCIA	CW	3	79.3 ± 3.1	92.0	84.8
GaRCIA	CW	3	83.8 ± 2.4	97.6	87.5
GaRCIA	LC	5	82.0 ± 3.5	98.4	**89.2**

train the model for 50 epochs on three, while evaluating it on the remaining fold for stratified cross-validation purposes. This gives us 4 scores that measure the performance of the hyper-parameters on the validation set. As there are many hyper-parameter combinations that are considered, we only report the top three performing parameter settings for each algorithm as found on the validation set.

For comparison we keep the following hyper-parameters for the experiments: learning rates for the prototypes, transformations and filter parameters are set to 0.1, 0.01 and 0.05 respectively. In the stratified cross-validation the following hyper-parameters are grid searched: the number of prototypes per class (1 through 5) and whether or not local (LC), class-wise (CW) or global (GL) $\mathbf{\Omega}$ matrices are used. In the case of the Gabor filter bank (static or otherwise) a sum of 16 Gabor filters is used which are initialized using $\mathbf{\Theta}_l^j = \{\theta, \lambda, 0, 2.4, \frac{3}{4}\}$ with $\theta \in \{0, \frac{22.5\pi}{180}, \frac{45\pi}{180}, \frac{67.5\pi}{180}, \frac{\pi}{2}, \frac{112.5\pi}{180}, \frac{135\pi}{180}, \frac{157.5\pi}{180}\}$ and $\lambda \in \{5, 5\sqrt{2}\}$. From an empirical sensitivity analysis we found that small changes of θ resulted in unstable learning. Therefore, we exclude the θ parameter from adaptation and create the filter bank using fixed and equally spaced θ values between 0 and 2π.

The results are summarized in Table 1. It is clear that the use of adaptive filter banks is fruitful as all models adapting them outperform the version in which it is kept static (first row). While the GaRCIA model has much less parameters than RCIA, there are no obvious performance differences between them on the validation and train set. Furthermore, the GaRCIA model performs slightly better on the hold-out test set suggesting that the learned Gabor filters improve generalization. A learned filter bank of the brick class, that excites to horizontal and vertical lines often present in brick textures, is shown in Fig. 2e.

4 Conclusion

In this contribution we introduce the use of adaptive Gabor filters into the interpretable machine learning domain by presenting the novel adaptive Gabor real-valued color image analysis LVQ algorithm (GaRCIA-LVQ). The adaptive Gabor filter extension typically reduces the number of parameters for optimization, since each individual filter exhibits only 5 parameters as compared to the general convolution that resembles the size of the patches considered. First experiments with Vistex color texture images show promising results with the adaptive filters outperforming the base RCIA-LVQ model, despite using much

ESANN 2022 proceedings, European Symposium on Artificial Neural Networks, Computational Intelligence and Machine Learning. Bruges (Belgium) and online event, 5-7 October 2022, i6doc.com publ., ISBN 978287587084-1. Available from http://www.i6doc.com/en/.

less parameters and preserving the structure of Gabor functions in the filter bank. The trained class-specific Gabor filters can be readily interpreted, and the obtained filter parameters inspected with respect to their meaning for detected structure of each class. In future work we will investigate different dissimilarities based on weighted trainable combinations of class-specific color channel Gabor responses and extensions to combined filters for more complicated structures.

References

[1] Marcelja and Stjepan. Mathematical description of the response of simple cortical cells. *Journal of the Optical Society of America*, 70:1297–300, 12 1980.

[2] J. J. Kulikowski and P. O. Bishop. Fourier analysis and spatial representation in the visual cortex. *Experientia*, 37(2):160–163, Feb 1981.

[3] D. M. MacKay. Strife over visual cortical function. *Nature*, 289(5794):117–118, Jan 1981.

[4] T. M. Caelli. Facilitative and inhibitory factors in visual texture discrimination. *Biological Cybernetics*, 39(1):21–26, Nov 1980.

[5] J. P. Jones and L. A. Palmer. An evaluation of the two-dimensional gabor filter model of simple receptive fields in cat striate cortex. *Journal of Neurophysiology*, 58(6):1233–1258, 1987. PMID: 3437332.

[6] A. G. Ramakrishnan, S. Kumar Raja, and H. V. Raghu Ram. Neural network-based segmentation of textures using gabor features. In *Proc. of the 12th IEEE Workshop on Neural Networks for Signal Processing*, pages 365–374, 2002.

[7] M. Lindenbaum and R. S. Gabor filter analysis for texture segmentation. In *Proc. of the 2006 (CVPRW'06)*, page 178, 2006.

[8] L. Chen, G. Lu, and D. Zhang. Effects of different gabor filters parameters on image retrieval by texture. In *Proc. of the 10th International Multimedia Modelling Conference*, pages 273–278, 2004.

[9] C. Mandriota, M. Nitti, N. Ancona, E. Stella, and A. Distante. Filter-based feature selection for rail defect detection. *Machine Vision and Applications*, 15(4):179–185, 2004.

[10] C. Olah, N. C., L. S., G. G., M. P., and S. C. An overview of early vision in inceptionv1. *Distill*, 2020. `https://distill.pub/2020/circuits/early-vision`.

[11] A. Krizhevsky, I. Sutskever, and G. E. Hinton. Imagenet classification with deep convolutional neural networks. In *Proc. of the 25th International Conference on Neural Information Processing Systems*, NIPS12, pages 1097–1105. Curran Associates Inc., 2012.

[12] C Szegedy, W Liu, Y Jia, P Sermanet, S E. Reed, D Anguelov, D Erhan, V Vanhoucke, and A Rabinovich. Going deeper with convolutions. *CoRR*, abs/1409.4842, 2014.

[13] K He, X Zhang, S Ren, and J Sun. Deep residual learning for image recognition, 2015.

[14] G Huang, Z Liu, L van der Maaten, and K Q. Weinberger. Densely connected convolutional networks, 2016.

[15] Y. Yuan, J. Zhang, and Q. Wang. Deep gabor convolution network for person re-identification. *Neurocomputing*, 378:387–398, 2020.

[16] Y Zhang, W L, L Zhang, X Ning, L Sun, and Y Lu. Adaptive learning gabor filter for finger-vein recognition. *IEEE Access*, 7:159821–159830, 2019.

[17] K. Bunte, P. Schneider, B. Hammer, F. Schleif, T. Villmann, and M. Biehl. Limited rank matrix learning, discriminative dimension reduction and visualization. *Neural Networks*, 26:159–173, 2012.

[18] K. Bunte, I. Giotis, N. Petkov, and M. Biehl. Adaptive Matrices for Color Texture Classification. In *14th International Conference on Computer Analysis of Images and Patterns (CAIP)*, volume 6855 of *Lecture Notes in Computer Science*, pages 489–497, Seville, Spain, "Aug." 2011.

[19] I. Giotis, K. Bunte, N. Petkov, and M. Biehl. Adaptive matrices and filters for color texture classification. *Journal of Mathematical Imaging and Vision*, 47(1):79–92, 2013.

[20] P. Kruizinga and N. Petkov. Nonlinear operator for oriented texture. *IEEE transactions on image processing*, 8(10):1395–1407, October 1999.

[21] Massachusetts Institute of Technology. Database VisTex of color textures from MIT. `https://vismod.media.mit.edu/vismod/imagery/VisionTexture/vistex.html` Online; accessed 8-August-2021.